

# On a deep connection between factorization and saturation: new insight into modeling high-energy proton-proton and nucleus-nucleus scattering in the EPOS4 framework

K. Werner

January 31, 2023

SUBATECH, Nantes University – IN2P3/CNRS – IMT Atlantique, Nantes, France

## Abstract

Following very elementary time-scale arguments, we know that multiple nucleon-nucleon scatterings in high-energy nucleus-nucleus (AA) collisions or multiple partonic scatterings in proton-proton (pp) collisions must happen in parallel. However, a parallel scattering formalism does not automatically lead to inclusive cross sections showing factorization in pp or binary scaling in AA scatterings. We will report on new ideas (leading to EPOS4), which will provide some new understanding of a deep connection between four basic concepts in pp and AA collisions: parallel scattering, energy conservation, factorization, and saturation. Missing one will spoil the whole picture. From a practical point of view, we can compute within the EPOS4 framework parton distribution functions (EPOS PDFs) and use them to compute inclusive pp cross sections. So for the first time, we may compute inclusive jet production (for heavy or light flavors) at very high transverse momentum ( $p_t$ ) and at the same time in the same formalism study flow effects at low  $p_t$  in high-multiplicity pp events, making EPOS4 a full-scale "general purpose event generator". We discuss applications, essentially multiplicity dependencies (of particle ratios, mean  $p_t$ , charm production) which are very strongly affected by the saturation issues discussed in this paper.

## 1 Some introductory remarks about factorization, parallel scattering, and saturation

Two major discoveries made it possible to reliably compute cross sections in high-energy proton-proton (pp) scattering. There is first of all the fact that the coupling constant  $\alpha_s$  of strong interactions becomes weaker with increasing scale, referred to as "asymptotic freedom" [1, 2], which allows the use of perturbation theory to compute parton-parton cross sections. The other crucial issue is called "factorization" [3, 4], which amounts to separating short- and long-distance physics at some "factorization scale"  $\mu$ , which allows to write the inclusive pp cross section as a convolution of two parton distribution functions (PDFs) and a (calculable) elementary parton-parton cross section. The PDFs contain all the long-distance physics, below the scale  $\mu$ . Factorization in connection with asymptotic freedom turned out to be an extremely powerful concept, with numerous important applications. Extended to collisions of two nuclei, composed of  $A$  and  $B$  nucleons, factorization means that the cross section for rare processes is given ad  $AB$  times the pp cross section. This is usually referred to as "binary scaling".

Factorization is an impressive tool, being very useful when it comes to studying inclusive particle production, but there are very interesting cases not falling into this category, like high-multiplicity events in proton-proton scattering in the TeV energy range, where a very large number of parton-parton scatterings contribute. Such events are particularly interesting, since the CMS collaboration observed long-range near-side angular correlations for the first time in high-multiplicity proton-proton collisions [5], which was before considered to be a strong signal for collectivity in heavy ion collisions. And studying such high-multiplicity events (and multiplicity dependencies of observables) goes much beyond the frame covered by factorization. Here we need an appropriate tool, able to deal with multiple scatterings.

The most important fact about multiple parton-parton scatterings: they must occur in parallel, and not sequentially, as we are going to justify in the following. We know that parton-parton scatterings are preceded by a series of successive parton emissions according to DGLAP evolution equations [6, 7, 8]. In particular, the first emitted partons carry a large momentum corresponding to a large  $\gamma$  factor, so they are "long-lived" particles. Correspondingly, the whole reaction takes a long time, which makes it impossible to have two (or more) successive parton-parton scatterings. Multiple scattering must therefore

happen in parallel. In the case of nucleus-nucleus scattering, the nucleon-nucleon collisions also happen in parallel, and this is simply due to the fact that at very high energies, the “reaction time” (the time it takes for the two nuclei to pass through each other) is much shorter than the particle formation time. So first all the interactions are realized (instantaneously) and particle production comes later. We have a “double parallel scattering” scenario: the nucleon-nucleon scatterings happen in parallel, and for each nucleon-nucleon scattering, the parton-parton collisions occur in parallel.

There is another important issue in high-energy scattering: with increasing energy, partons with very small momentum fractions  $x \ll 1$  become increasingly important, since the PDFs at small  $x$  become large. This means that the parton density becomes large, and therefore the linear DGLAP evolution scheme is not valid anymore, non-linear evolution takes over, considering explicitly gluon-gluon fusion. These phenomena are known as “small  $x$  physics” or “saturation” [9, 10, 11, 12, 13, 14, 15, 16, 17, 18, 19, 20, 21, 22], the main effect being a screening of low transverse momentum ( $p_t$ ) particle production (below a “saturation scale”). Without saturation, both total cross sections and multiplicities would explode at high energies. Saturation effects are expected to be even stronger in nucleus-nucleus collisions, simply because gluon ladders emitted from different nucleons may fuse.

Factorization (= binary scaling in case of AA), saturation, and parallel multiple scattering are clearly important issues in high-energy scattering. What we are going to show in this paper: they are very closely connected. But this can only be seen when the parallel scattering respects rigorously energy conservation. It is tempting to consider some “high-energy limit” and ignore energy conservation, all formulas become much simpler, but this will spoil the picture, as we will show. So finally, there is a deep connection between factorization, energy conservation, parallel scattering, and saturation, see Fig. 1.

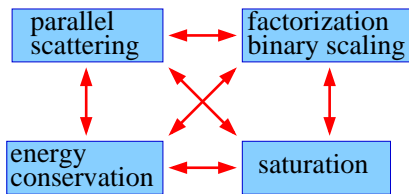


**Figure 1:** Factorization, energy conservation, parallel scattering, and saturation: four concepts being deeply connected.

A proper theoretical treatment needs to consistently accommodate these four crucial concepts, and this is realized in the EPOS4 project, whereas earlier versions were never able to do so.

## 2 EPOS4 S-matrix approach

We first consider pp scattering. An appropriate tool to implement parallel scatterings is provided by S-matrix theory, see [23] and references therein, as [24, 25, 6, 26], where multiple parallel scatterings can be implemented in a simple and transparent fashion. Factorization and binary scaling are not “assumed”, they must come out! The S-matrix is per definition the representation  $S_{ij} = \langle i | \hat{S} | j \rangle$  of the scattering operator  $\hat{S}$  using some basis of asymptotic states, and the corresponding T-matrix is defined via  $S_{fi} = \delta_{fi} + i(2\pi)^4 \delta(p_f - p_i) T_{fi}$ . Particularly important is the diagonal element,  $T_{ii}$ , representing elastic scattering, where the asymptotic state  $|i\rangle$  corresponds to two incoming protons. Assuming purely transverse momentum transfer, one may Fourier transform  $T_{ii}$  with respect to the transverse momentum exchange  $\vec{k}$  to obtain some function  $T(s, b)$ , with the Mandelstam variable  $s$  and the impact parameter  $b$ , in the following simply named “T-matrix”  $T$ .

The EPOS4 S-matrix approach is based on the hypothesis that the T-matrix  $T$  can be written as a sum of products of “elementary” T-matrices  $T_{\text{Pom}}$ , the latter ones representing parton-parton scattering by exchanging a “Pomeron” (without specifying its nature for the moment), as

$$iT = \sum_{n=0}^{\infty} \int dX \frac{1}{n!} V \times \{iT_{\text{Pom}} \times \dots \times iT_{\text{Pom}}\} \times V, \quad (1)$$

with the “vertex”  $V$  representing the connection to the projectile and target remnants. The symbol  $X$  stands for all integration variables, to be specified in the following. In Fig. 2, we show a graphical representation of a double

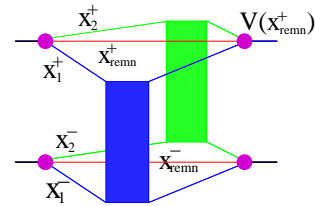


**Figure 2:** Double scattering diagram.

scattering ( $n = 2$ ), where the blue and green boxes are the elementary T-matrices  $T_{\text{Pom}}$ , representing parton-parton scattering, and the magenta dots are the vertices  $V$ . The elementary T-matrices are characterized by the light-cone momentum fractions  $x^\pm$  of the incoming partons, in addition to  $s$  and  $b$ . The precise content of the Pomerons (boxes) and the functional dependencies on these variables will be discussed later, the general discussion in this chapter does not depend on these details. The vertices depend on the light-cone momentum fractions of the remnants, i.e.  $x_{\text{remn}}^+$  (projectile side) or  $x_{\text{remn}}^-$  (target side). The vertices assure energy-momentum conservation via

$$x_{\text{remn}}^\pm = 1 - \sum x_i^\pm, \quad (2)$$

which will be crucial for the discussions in this paper. The integration  $\int dX$  amounts to integrating over all light-cone momentum fractions. Each term (for  $n > 1$ ) in the sum of eq. (1) represents multiple scatterings happening in parallel, as it should be.

The generalization of our multiple parallel scattering picture towards nucleus-nucleus (AA) collisions (including proton-nucleus) is trivial, one simply writes a product of pp expressions,

$$iT = \int dX \prod_{i=1}^A V \prod_{k=1}^{AB} \left\{ \sum_{n_k=0}^{\infty} \frac{1}{n_k!} \{iT_{\text{Pom}} \times \dots \times iT_{\text{Pom}}\} \right\} \prod_{j=1}^B V, \quad (3)$$

for colliding two nuclei with mass numbers  $A$  and  $B$ . Here, we have one vertex  $V$  per remnant, and a sum of products of elementary T-matrices per nucleon-nucleon pair. This formula does NOT mean at all a sequence of pp collisions, they are perfectly happening in parallel. The integration  $\int dX$  here means integration over all light-cone momentum fractions and over all transverse position of the nucleons. The generalization eq. (3) is conceptually trivial, but it should be noted that we have (for big nuclei) 10000000 dimensional non-separable integrals.

So far we discussed only elastic scattering, for pp and AA, the connection with inelastic scattering provides the “optical theorem”, which is at high energy given as

$$2s \sigma_{\text{tot}} = \frac{1}{i} \text{disc } T \equiv \text{cut } T, \quad (4)$$

with  $\text{disc } T$  being the s-channel discontinuity  $T(s + i\epsilon) - T(s - i\epsilon)$ . So we need to compute the “cut” of the complete diagram,  $\text{cut } T$ , i.e. for pp we need to evaluate

$$\text{cut} \{V \times iT_{\text{Pom}} \times \dots \times iT_{\text{Pom}} \times V\}. \quad (5)$$

Cutting a multi-Pomeron diagram corresponds to the sum of all possible cuts, considering, in particular, all possibilities of cutting or not any of the parallel Pomerons, so we have finally sums of products with some fraction of the Pomerons being cut (“cut Pomerons”), the others not (“uncut Pomerons”). An uncut Pomeron is by definition the sum of two contributions, the Pomeron being to the right or to the left of the cut. Since cut and uncut Pomerons have opposite signs, we get big sums of positive and negative terms, with plenty of interference and cancellations, which absolutely crucial for understanding these collisions. In Fig. 3, we show the sum of all possible cuts of a two-Pomeron diagram, not considering remnants for simplicity.

Let us consider a simple example of a realization of a Pomeron (the real one is much more complicated), namely a simple parton ladder with two gluon and two quark ladder rungs, see fig. 4. The cut is represented by a vertical red dashed line. For a cut diagram, the Feynman rules are modified in the sense that all elements to the left of the cut are treated normally, for all elements to the right one takes the complex conjugate of the normal result, and all propagators crossing the cut line are

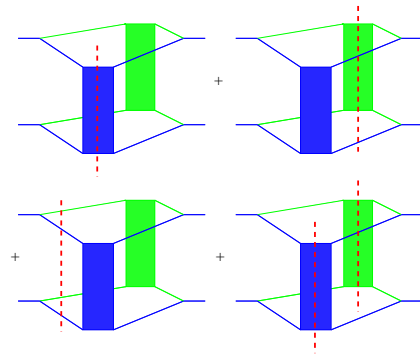


Figure 3: Sum of all possible cuts of a two-Pomeron diagram.

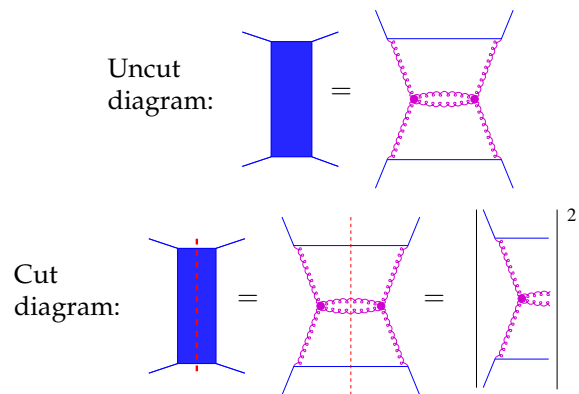
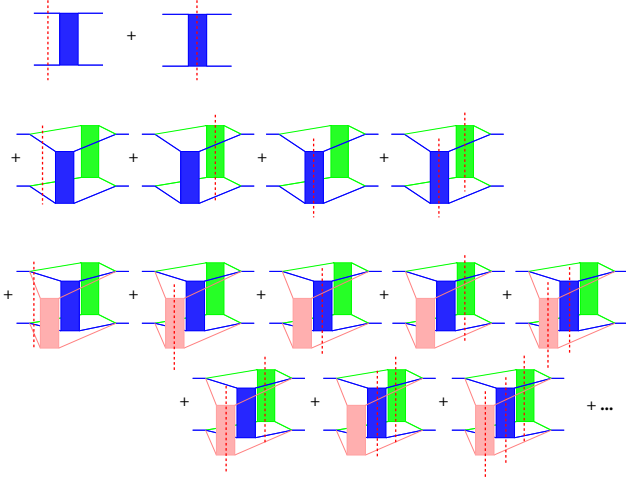


Figure 4: A simple example of an uncut and the corresponding cut diagram.

replaced by a mass shell condition  $\delta(p^2 - m^2)$ . The cut diagram corresponds therefore to an inelastic amplitude squared, with all particles on the cut line being final on-shell particles. This is not only true for this simple example but always. So the notion of cut diagrams is very useful, in particular for multiple scattering scenarios.

We come back to the general discussion, where the precise structure of Pomeron is not (yet) known. All the diagrams which contribute to  $\text{cut } T$  (and therefore to the inelastic cross section) in pp represent an infinite series, composed of all possible cut and uncut Pomerons (boxes) as shown in Fig. 5 up to order  $n = 3$ .

Let us consider inclusive cross sections, like jet cross sections or particle production cross section, where  $n$ -Pomeron events contribute on average  $n$  times more than single Pomeron events. Ignoring (for a moment) energy-momentum conservation by simply removing the vertices  $V$ , the calculations simplify enormously, and one can prove that at each order beyond  $n = 1$ , the sum of all possible cuts cancel, referred to as AGK cancellations [26], and therefore, for inclusive cross sections and only for those, only the single Pomeron events contribute, as indicated in Fig. 6. If a Pomeron is considered to be a parton ladder, with parton evolutions from both sides and a hard elementary parton-parton scattering in the middle, we can write the inclusive pp cross section as a convolution of two parton distribution functions and a (cal-



**Figure 5:** All the diagrams which contribute to cut  $T$ .

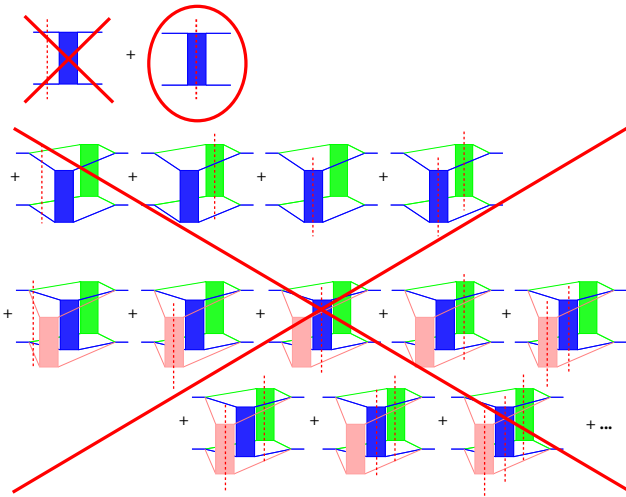


**Figure 6:** Cancellations for inclusive cross sections, when energy-momentum conservation is ignored.

culable) elementary parton-parton cross section, which amounts to factorization! So factorization here is the result of a huge amount of cancellations. For completeness, also for inclusive cross sections in AA scattering we observe this phenomenon of cancellations, such that finally only a single Pomeron contributes, and the cross section turns out to be  $AB$  times the proton-proton cross section, which is nothing but “binary scaling”.

So we get factorization / binary scaling for inclusive cross sections, but we get it ALWAYS and not only for hard processes (like high  $p_t$  particle production) as it should be, so ignoring energy-momentum conservation is not the solution, and we better keep it. But then “cancellation issues” become complicated. The difficulty is

- to keep all diagrams
- make sure that they cancel where they should do so: for inclusive cross sections, for “hard probes”
- make sure that energy conservation does not spoil

factorization in that case (like in EPOS LHC [27])

To achieve this, the precision concerning the pQCD calculations is an important issue, to be reported in a separate publication, and one needs a good strategy to implement saturation in order to cure the factorization issues spoiled by energy-momentum conservation. We first need to understand in which way the latter affects factorization. Let us consider a particular Pomeron in AA collisions (including pp as a special case), connected to projectile nucleon  $i$  and target nucleon  $j$ , see fig. 7. There might be

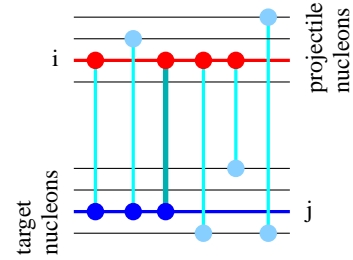


**Figure 7:** A Pomeron connected to projectile nucleon  $i$  and target nucleon  $j$ , together with other Pomerons connected to one (or both) of these nucleons.

other Pomerons, connected to one (or both) of these nucleons. The corresponding Pomeron-nucleon connections are marked as red and blue dots. It is obvious that the additional Pomerons connected to the same nucleons  $i$  and  $j$  compete with each other, they have to share the initial energy-momentum of the two nucleons. The more Pomerons are connected, the less energy is available for one particular Pomeron. To quantify this statement, we define the “connections number”

$$N_{\text{conn}} = \frac{N_P + N_T}{2}, \quad (6)$$

with  $N_P$  being the number of Pomerons connected to  $i$ , and with  $N_T$  being the number of Pomerons connected to  $j$  (the variable  $N_{\text{conn}}$  corresponds to half of the number of red and blue points in fig. 7). We only consider cut Pomerons here, since the uncut ones represent elastic scatterings. The case  $N_{\text{conn}} = 1$  corresponds to an isolated Pomeron, which may take all the energy of the initial nucleons, whereas in case of  $N_{\text{conn}} > 1$  the energy will be shared. Let us consider, for a given Pomeron, the “Pomeron energy fraction”

$$x_{\text{PE}} = x^+ x^- = \frac{M_{\text{Pom}}^2}{s}, \quad (7)$$

with light-cone momentum fractions  $x^\pm$ , and with  $M_{\text{Pom}}$  being the transverse mass of the Pomeron, so the distribution  $f(x_{\text{PE}})$  of the variable  $x_{\text{PE}}$  characterizes the energy distribution of the Pomerons, and the distribution obviously depends on  $N_{\text{conn}}$ , so we use the notation  $f^{(N_{\text{conn}})}(x_{\text{PE}})$ . The reference distribution is  $f^{(1)}(x_{\text{PE}})$ , which is the  $x_{\text{PE}}$  distribution for isolated Pomerons, like for pp scatterings with only one Pomeron involved. Since

we expect for  $N_{\text{conn}} > 1$  a “deformation” of the the  $x_{\text{PE}}$  distributions due to energy-momentum conservation, we define the ratio

$$R_{\text{deform}} = \frac{f^{(N_{\text{conn}})}(x_{\text{PE}})}{f^{(1)}(x_{\text{PE}})}, \quad (8)$$

called “deformation function”. This function will be computed in an iterative fashion: starting from some “initial guess”, one uses this  $R_{\text{deform}}$  to define our Pomerons (to be discussed later), then one uses these Pomerons to compute cross sections which (among other things) allow computing  $R_{\text{deform}}$ , which is then used to redefine the Pomerons and compute an improved  $R_{\text{deform}}$  and so on. The procedure converges very fast. In practice, we have found a very simple functional form for this function which accommodates all systems, centrality classes, and energies. We determine (with few iterations) and tabulate the parameters, and then use parameterized deformation functions. In Fig. 8, we show as an example the

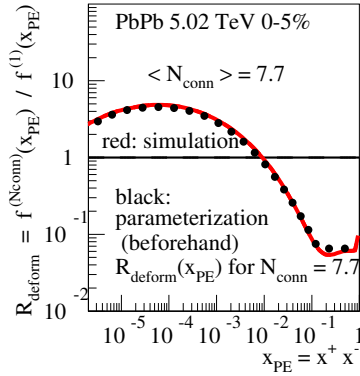


**Figure 8:** Deformation function (see text) for the centrality class 0-5% in PbPb collisions at 5.02 TeV.

deformation function for the centrality class 0-5% in PbPb collisions at 5.02 TeV, with an average value of  $N_{\text{conn}}$  of roughly 7.7. We plot the parameterized function (black dots) and the “computed distribution” which comes out after a full simulation (red curve). The two curves indeed agree, which means that we are able to correctly predict the deformation. The functional form is as we expect, large  $x^\pm$  values (close to unity) are suppressed, and small  $x^\pm$  values are increased. And the effect is big, the suppression in the interval  $[0.1, 1]$  is roughly  $1/20$ .

With the deformation being under control, we can define the “box”, called “cut Pomeron” and named  $G$ . The latter depends on the light-cone momenta  $x^\pm$ , the energy squared  $s$ , and the impact parameter  $b$ , so we use  $G(x^+, x^-, s, b)$ , see Fig. 9. On the other hand (and here comes the link to QCD), we have the “cut ladder”  $G_{\text{QCD}}$ , corresponding to a cut parton ladder based on DGLAP parton evolutions from the projectile and target side, with an elementary QCD cross section in the middle [23]. The cut ladder  $G_{\text{QCD}}$  depends as well on  $x^\pm$ ,  $s$ , and  $b$ , and in addition there is the crucial parameter  $Q_0^2$  being the

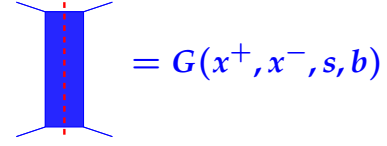


**Figure 9:** The cut Pomeron  $G$ .

low virtuality cutoff in the DGLAP evolution, so we use the notation  $G_{\text{QCD}}(Q_0^2, x^+, x^-, s, b)$ . Whereas the cutoff is usually a constant of the order of  $1 \text{ GeV}^2$ , we consider it as a variable that may take any value, and we compute and tabulate  $G_{\text{QCD}}(Q^2, x^+, x^-, s, b)$  for large ranges of discretized values of all five arguments, such that  $G_{\text{QCD}}$  can be computed via interpolation for any choice of the arguments. In earlier EPOS version, we simply assumed  $G$  to be equal to  $G_{\text{QCD}}$ , which completely spoils factorization.

The EPOS4 procedure goes as follows:

For each cut Pomeron, for given  $x^\pm$ ,  $s$ , and  $b$ , and for a given functional dependence  $G_{\text{QCD}}(Q^2, x^+, x^-, s, b)$  with  $G_{\text{QCD}}$  = “DGLAP parton ladder” with a low virtuality cutoff  $Q^2$ , we postulate:

$$G(x^+, x^-, s, b) = \frac{n}{R_{\text{deform}}(x_{\text{PE}})} G_{\text{QCD}}(Q_{\text{sat}}^2, x^+, x^-, s, b), \quad (9)$$

with  $n$  being a normalization constant, not depending on  $x^\pm$ . It may depend on  $N_{\text{conn}}$ , as do  $R_{\text{deform}}$  and  $Q_{\text{sat}}^2$ . Considering a large value of  $N_{\text{conn}}$ , we have as output a deformed  $x_{\text{PE}}$  distribution, but the input function  $G$  contains  $1/R_{\text{deform}}$  and so the deformation cancels out, always, even for large deformations. In that case, the saturation scale may become big. This is the crucial feature: although energy-momentum conservation “deforms” the  $x_{\text{PE}}$  distributions for large  $N_{\text{conn}}$ , the distribution is given by  $G_{\text{QCD}}(Q_{\text{sat}}^2, x^+, x^-, s, b)$ , which does not depend on  $N_{\text{conn}}$ , apart of the implicit  $N_{\text{conn}}$ -dependence of  $Q_{\text{sat}}^2$  – representing thus a “dynamical saturation scale”. On the other hand, the saturation scale affects small  $p_t$  particle production, whereas large  $p_t$  is not touched.

From this discussion, it becomes clear that for any number of  $N_{\text{conn}}$ , the inclusive particle production is governed by a single Pomeron represented by  $G_{\text{QCD}}$ , and the  $p_t$  dependence of outgoing partons will be independent of  $N_{\text{conn}}$  in the hard domain (high  $p_t$ ). Computing  $p_t$  distribution according to  $G_{\text{QCD}}$  amounts precisely to factorization or binary scaling in AA scattering, but - again - only obtained for hard processes. In other words, computing  $R_{\text{AA}}$  in a full AA simulation, we get unity at large  $p_t$ .

So we have shown that in a parallel scattering scenario (which is mandatory at high energies), energy-momentum conservation, saturation, and factorization / binary scaling are strongly connected, as sketched in Table 1. As shown earlier, turning off energy-momentum

energy conservation	dynamical saturation	resulting $R_{AA}$ vs pt	
No	No	= 1 everywhere	✗
Yes	No	< 1 everywhere	✗
Yes	Yes	< 1 at small pt = 1 at large pt	✓

**Table 1:** Energy-momentum conservation and saturation affect factorization / binary scaling, the latter expressed via  $R_{AA}$ . (✗=“wrong”, ✓=“right”)

conservation without any saturation prescription, we get  $R_{AA} = 1$  everywhere (wrong), whereas turning on energy-momentum conservation but still without any saturation prescription, we get  $R_{AA} \ll 1$  (wrong again). What made the approach work is a “dynamical saturation”, such that the saturation scale “absorbs” all the deformation due to energy-momentum conservation.

Whereas eq. (9) seems to be the crucial relation, which allows to accommodate energy-momentum conservation, saturation, and factorization, there are two ways to use it. One may assume some functional form of  $Q_{\text{sat}}^2(N_{\text{conn}}, x_{\text{PE}})$ , as in in [28] (our first use of a dynamical saturation scale), or use a parameterization of  $G$  and obtain  $Q_{\text{sat}}^2$ , proposed in [29], but at the time we did not understand the role of the deformation. In EPOS4, we parameterize  $G$ . One starts with the (very reasonable) assumption that  $G$  has a “Regge-pole structure” as  $G \propto \alpha x_{\text{PE}}^\beta$ , where the  $s, b$  dependence of  $\alpha$  and  $\beta$  is parameterized with the parameters being fixed by compar-

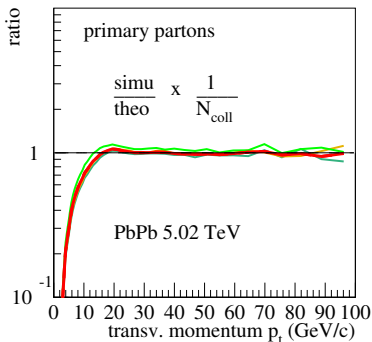


**Figure 10:** The inclusive  $p_t$  distribution of partons for a full simulation (simu) divided by  $N_{\text{coll}}$  and the “reference curve” (theo), which is the corresponding distribution for a single Pomeron, calculated analytically. We show results for minimum bias PbPb collisions at 5.02 TeV (red curve) as well as results for different centrality classes.

ing simulation results to basic experimental data. In this way, the l.h.s. of eq. (9) is known, and the equation then defines and allows to calculate  $Q_{\text{sat}}^2$  for given  $N_{\text{conn}}$ .

As a first result of EPOS4 simulations, we are going to show that factorization / binary scaling really works in practice. In Fig. 10, we show the inclusive  $p_t$  distribution of partons for a full simulation (simu) divided by  $N_{\text{coll}}$  and the “reference curve” (theo), which is the cor-

responding distribution for a single Pomeron, calculated analytically. We show results for minimum bias PbPb collisions at 5.02 TeV (red curve) as well as results for different centrality classes. One can see that the ratio is close to one for large values of  $p_t$ , whereas low  $p_t$  values are suppressed. Also in pp, the full simulation over the “reference curve” (single Pomeron) is close to unity at large  $p_t$  and comparing pp and AA, we get  $R_{AA} \approx 1$ .

### 3 EPOS4 factorization mode (single Pomeron) and EPOS4 PDFs

Since in the case of inclusive spectra at large  $p_t$  everything can be reduced to the single Pomeron case, we may use “a shortcut” and compute inclusive particle production simply by using a single Pomeron, without any need to use complicated Monte Carlo procedures. This is referred to as “EPOS4 factorization mode”. In this case, we simply need to evaluate the cut single Pomeron diagram, see Fig. 11. It is composed of a parton ladder with par-

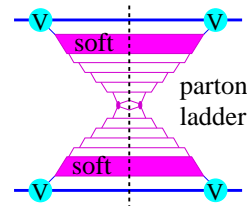


**Figure 11:** Cut single Pomeron diagram.

ton evolutions ( $E_{\text{QCD}}$ ) from both sides and an elementary QCD Born process in the middle ( $\sigma_{\text{QCD}}$ ), and the vertices  $V$ . In addition, the QCD parton evolution is preceded by a soft evolution ( $E_{\text{soft}}$ ). The complete expression is a convolution of several elements  $V \otimes E_{\text{soft}} \otimes E_{\text{QCD}} \otimes \sigma_{\text{QCD}} \otimes E_{\text{QCD}} \otimes E_{\text{soft}} \otimes V$ , which may be regrouped in several ways. One possibility is to convolute first the vertex, the soft evolution, and the QCD evolution on the projectile side, representing the parton distribution function (PDF) of the projectile, and correspondingly on the target side. The two PDFs represent actually the upper and lower part of the graph in Fig. 11, excluding the Born process. One computes (and tabulates) the PDFs  $f_{\text{PDF}}^k(x, \mu_F^2)$ , with  $x$  being the light-cone momentum fraction of the parton of flavor  $k$  entering the Born process, and  $\mu_F^2$  being the factorization scale. After this preparation, one may express the di-jet cross section (where di-jet simply refers to the two outgoing partons of the Born process) in terms of the PDFs, as

$$E_3 E_4 \frac{d^6 \sigma_{\text{dijet}}}{d^3 p_3 d^3 p_4} = \sum_{kl} \int \int dx_1 dx_2 f_{\text{PDF}}^k(x_1, \mu_F^2) f_{\text{PDF}}^l(x_2, \mu_F^2) \frac{1}{32s\pi^2} \sum |\mathcal{M}^{kl \rightarrow mn}|^2 \delta^4(p_1 + p_2 - p_3 - p_4), \quad (10)$$

with  $p_{1/2}$  and  $p_{3/4}$  being the four-momenta of the incoming and outgoing partons, and  $\mathcal{M}^{kl \rightarrow mn}$  is the corresponding matrix element. In order to get the complete expression corresponding to Fig. 11, one needs to integrate  $\int \frac{d^3 p_3 d^3 p_4}{E_3 E_4}$  over the differential cross section eq. (10), whereas to obtain the inclusive jet (=parton) cross section one needs to integrate  $\frac{d^3 p_4}{E_4}$ . In any case, thanks to the four-dimensional  $\delta$  function, the remaining numerical integration is easily done. The single Pomeron shown in Fig. 11 is actually just one (the most important one) of

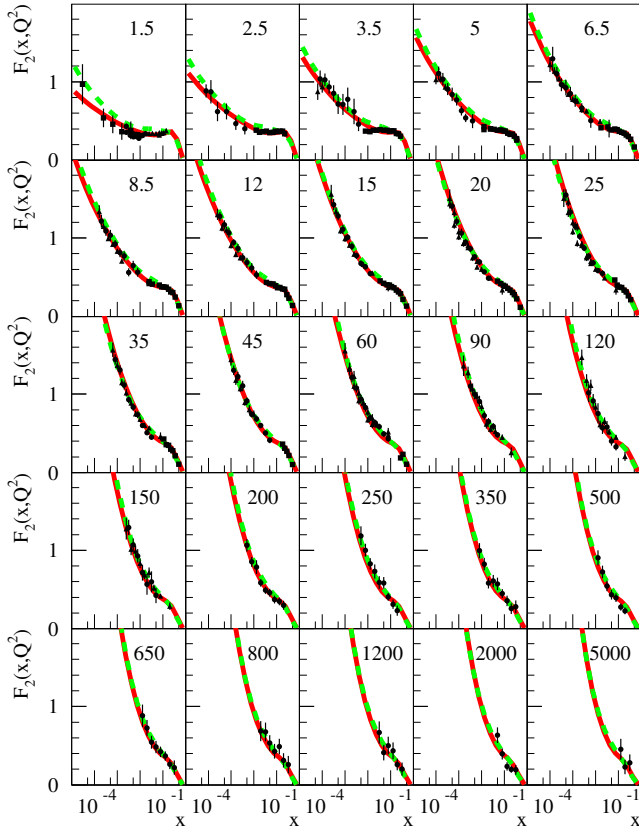


**Figure 12:**  $F_2$  as a function of  $x$  for different values of  $Q^2$ , the latter one indicated (in units of  $\text{GeV}^2$ ) in the upper right corners of each sub-plot. The red curve refers to EPOS PDFs, the green one to CTEQ PDFs, and the black points are data from ZEUS and H1.

several contributions, called “sea-sea” contribution, with a sea quark (after a soft evolution) being the first parton entering the partonic cascade on both sides. In addition, there is a “val-val” contribution, where valence quarks enter the partonic cascade, and correspondingly “val-sea” and “sea-val” contributions. Since the parton distribution function is just half of the Pomeron diagram, there are two contributions, the “sea” and a “val” one. For completeness, it should be said that in addition to the four Pomeron contributions based on “val” and “sea”, there is a fifth case, referred to as “soft”.

At least the quark parton distribution functions can be tested and compared with experimental data from deep

inelastic electron-proton scattering. The structure function  $F_2$  is given as  $F_2 = \sum_k e_k^2 x f_{\text{PDF}}^k(x, Q^2)$  with  $x = x_B = Q^2/(2pq)$ , with  $p$  being the momentum of the proton,  $q$  the momentum of the exchanged photon, and  $Q^2 = -q^2$ . In Fig. 12, we plot  $F_2$  as a function of  $x$  for different values of  $Q^2$ . The red curve refers to EPOS PDFs, the green one to CTEQ PDFs [30], and the black points are data from ZEUS [31] and H1 [32, 33, 34]. The two PDFs give very similar results, and both are close to the experimental data.

Having checked the EPOS PDFs, we will use these functions to compute the jet (parton) cross section, using eq. (10), integrating out the momentum of the second parton and the azimuthal angle of the first parton, for pp at 13 TeV. We define the parton yield  $dn/dp_t dy$  as the cross section, divided by the inelastic pp cross section, showing the result in Fig. 13. We show results based on

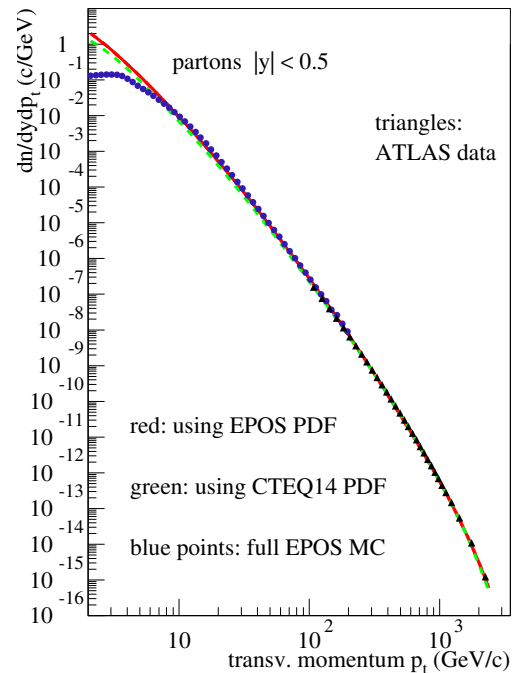


**Figure 13:** Parton yield  $dn/dp_t dy$  for pp at 13 TeV. We show results based on EPOS PDFs (red full line), CTEQ PDFs (green dashed line), the full EPOS simulation (blue circles), and experimental data from ATLAS (black triangles).

EPOS PDFs (red full line), CTEQ PDFs [30] (green dashed line), the full EPOS simulation (blue circles), and experimental data from ATLAS [35] (black triangles). At large values of  $p_t$ , all the different distribution agree, whereas at low  $p_t$  the EPOS Monte Carlo simulation results (using the full multiple scattering scenario) are significantly below the PDF results, as expected due to screening effects.

## 4 Full EPOS4 (core+corona, hydro, microcanonical decay): checking multiplicity dependencies

The “factorization mode” as discussed in the last section is very useful to investigate inclusive cross sections at high  $p_t$ . But this represents only a very small fraction of all possible applications, and there are very interesting cases outside the applicability of that approach. A prominent example, one of the highlights of the past decade in our domain, concerns “collective phenomena in small systems”, following many discoveries showing that high-multiplicity pp events show very similar “collective” features as earlier observed in heavy ion collisions [5]. High multiplicity means automatically “multiple parton scattering”, and as discussed earlier, this means that we have to employ the full parallel scattering machinery developed earlier, based on S-matrix theory.

But this is not the full story. The S-matrix part concerns “primary scatterings”, happening instantaneously at  $t = 0$ . As a result, in the case of a large number of Pomerons, we have correspondingly a large number of strings – which may overlap and “fuse”. In the EPOS framework, we employ a core-corona procedure [36, 37, 38], where the strings at a given proper time  $\tau_0$  are first cut into “string segments”, being separated into “core” and “corona” segments, depending on the energy loss of each segment when traversing the “matter” composed of all the other segments. Corona segment (per definition) can escape, whereas core segments lose all their energy and constitute what we call “core”, which acts as an initial condition for a hydrodynamic evolution [38]. The evolution of the core ends whenever the energy density falls below some critical value  $\epsilon_{FO}$ , which marks the point where the fluid “decays” into hadrons. It is not a switch from fluid to particles, it is a sudden decay, called “hadronization”. In EPOS4, we developed a new procedure of energy-momentum flow through the “freeze-out (FO) hypersurface” defined by  $\epsilon_{FO}$ , which allows defining an effective invariant mass, which decays according to microcanonical phase space into hadrons, which are then Lorentz boosted according to the flow velocities computed at the FO hypersurface. We also developed new and very efficient methods for the microcanonical procedure. All the technical details will be published separately, the aim of this paper is to present an overview and some important results. Summarizing the discussion in this paragraph, we have

- the “full” EPOS4 scheme, composed of
  - primary interactions, based on an S-matrix approach for parallel scatterings
  - secondary interactions, composed of
    - \* core-corona separation procedure
    - \* hydrodynamic evolution and microcanonical hadronization

\* hadronic afterburner (UrQMD [39, 40])

As an alternative, in order to better understand the different components, we also consider

- the “core+corona” (“co-co”) contribution, i.e. primary interactions + secondary interactions but without hadronic afterburner
- the “core” contribution, i.e. primary interactions + secondary interactions but without hadronic afterburner, only considering core particles
- the “corona” contribution, i.e. primary interactions + secondary interactions but without hadronic afterburner, only considering corona particles

We need to exclude in these cases the hadronic afterburner, because the latter affects both core and corona particles, so in the full approach, the core and corona contributions are not visible any more.

In the following, we will present particle ratios, always relative to pion yields, as well as mean  $p_t$  results, for the different contributions (“core”, “corona” etc), in pp and PbPb collisions at LHC energies. In all cases, the results depend strongly on the relative weight of core to corona. It is clear that for low multiplicity pp scattering corona will dominate, whereas for central PbPb collisions, the core will dominate. To be more quantitative, we compute the “core fraction”, defined as the ratio of core to core+corona for pion production (with pions being the most frequent particle species). In Fig. 14, we show re-

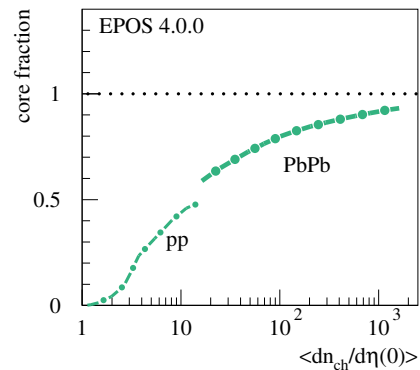


**Figure 14:** The “core fraction” for pp (thin lines) and PbPb scattering (thick lines).

sults for pp (thin lines) and PbPb (thick lines), and we see an almost continuous curve, going from zero (for low multiplicity pp) up to unity (for central PbPb). There is no overlap at intermediate multiplicity because we are running out of statistics for both pp and PbPb collisions. We consider actually pp at 7 TeV and PbPb at 2.76 TeV, since the particle ratios in the following refer to these energies.

In Fig. 15(left), we plot the ratio of  $\Omega$  baryon yields over  $\pi$  yields versus multiplicity. We show results for pp at 7 TeV (thin lines) and PbPb at 2.76 TeV (thick lines), compared to ALICE data [41, 42]. The different line styles



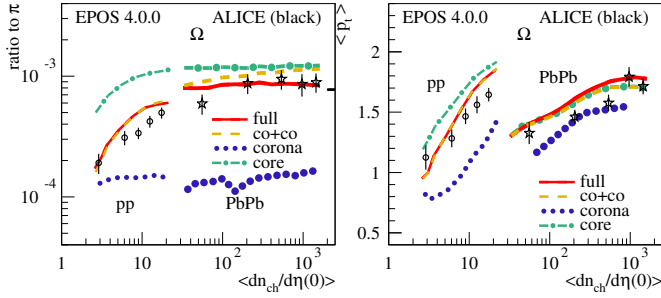


**Figure 15:** Ratio of  $\Omega$  over  $\pi$  (left plot) and average transverse momentum (right plot) versus multiplicity, for pp at 7 TeV (thin lines) and PbPb at 2.76 TeV (thick lines), compared to ALICE data.

refer to different contributions: the yellow dashed line refers to “core+corona” (“co-co”), i.e. primary interactions + hydro but without hadronic afterburner, the blue dotted line refers to the “corona” and the green dash-dotted line refers to “core” part. The red line is the “full” contribution, i.e. core + corona + hadronic afterburner. We see an almost flat line for the core contribution, similar for pp and PbPb, which is understandable, since “corona” means particle production from string fragmentation, which does not depend on the system. We observe also a flat curve for the “core” part at high multiplicity, which is again expected since the core hadronization is determined by the freeze-out energy density, which is system independent. However, when the system gets very small, we get a reduction of heavy particle production due to the microcanonical procedure (with its energy and flavor conservation constraints), whereas a grand canonical treatment would give a flat curve down to small multiplicities. It is remarkable that the “core” curve is far above the “corona” one, which simply reflects the fact that  $\Omega$  production is much more suppressed in string decay, compared to statistical (“thermal”) production. This explains why the “core+corona” contribution increases by one order of magnitude from low to high multiplicity, because simply the relative weight of the core fraction increases from zero to unity. The effect from hadronic rescattering (difference between “full” and “co-co”) is relatively small, some suppression due to baryon-antibaryon annihilation can be seen.

Whereas the  $\Omega$  over  $\pi$  ratios are essentially smooth curves, from pp to PbPb, the situation changes completely when looking at the average transverse momentum  $\langle p_t \rangle$  versus multiplicity, as shown in Fig. 15(right), where we also show results for pp (thin curves) and PbPb (thick curves), for the different contributions. Here we see (for all curves) a significant discontinuity when going from pp to PbPb. The “corona” contributions are not flat (as the ratios), but they increase with multiplicity, in the case of pp even more pronounced as for PbPb. This is a “saturation effect”: the saturation scale increases with multiplicity, which means with increasing multiplicity the events get harder, producing higher  $p_t$ . The situ-

ation is different for PbPb, where an increase of multiplicity is mainly due to an increase of the number of active nucleons, with a more modest increase of the saturation scale with multiplicity. Also the “core” curves increase strongly with multiplicity, and here as well more pronounced in case of pp, due to the fact that we get for high-multiplicity pp high energy densities within a small volume, leading to strong radial flow. Again,

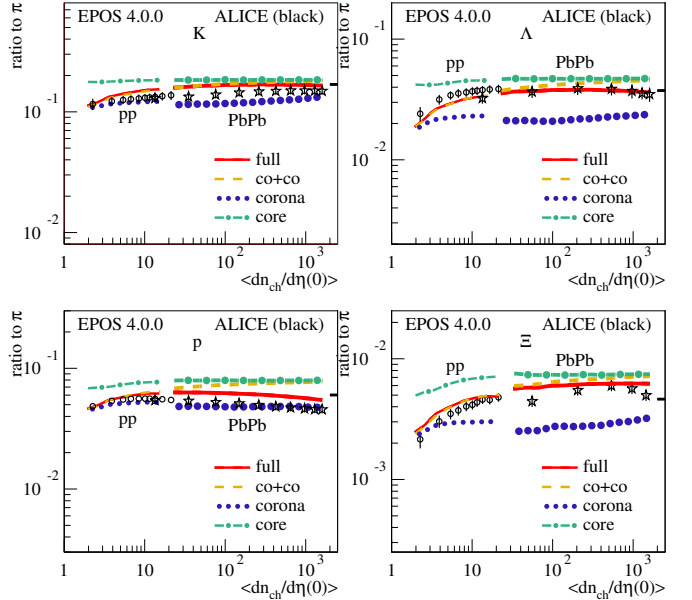


**Figure 16:** As fig. 15(left), but for  $K$ ,  $p$ ,  $\Lambda$ ,  $\Xi$ .

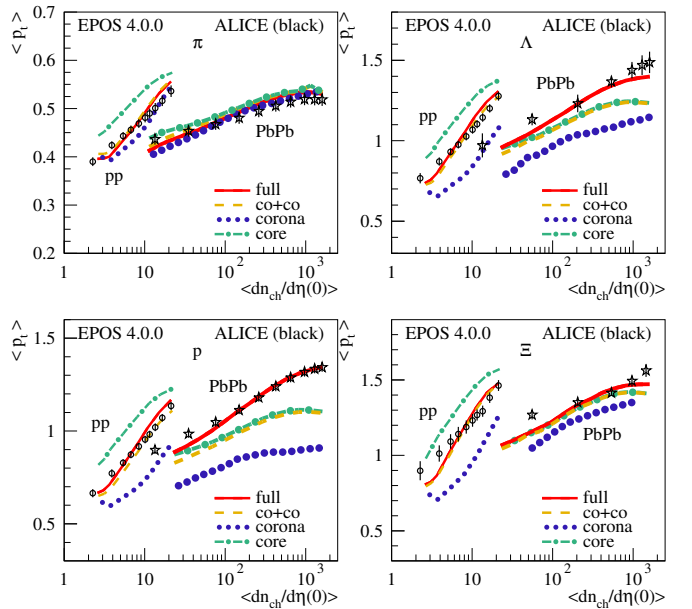


**Figure 17:** As fig. 15(right), but for  $K$ ,  $p$ ,  $\Lambda$ ,  $\Xi$ .

the core+corona contribution is understood based on the continuous increase of the core fraction from low to high multiplicity.

In Figs. 16 and 17, we show the multiplicity dependen-

cies of ratios and mean  $p_t$  for different hadrons, which are qualitatively similar to the  $\Omega$  results, just the difference between the corona and the core curves are smaller. The data are from ALICE [43, 44, 42, 45, 41].

It is very useful (and necessary) to consider at the same time the multiplicity dependence of particle ratios and of mean  $p_t$  results, since their behavior is completely different (the former is continuous, the latter jumps). Despite these even qualitative differences between the two observables, the physics issues behind these results is the same, namely saturation, core-corona effects which mix flow (being very strong) and non-flow, and microcanonical hadronization of the core.

Another very important and useful variable is the multiplicity dependence of  $D$  meson production, where “ $D$ ” stands for the sum of  $D^0$ ,  $D^+$ , and  $D^{*+}$ . This is much more than just “another particle”, since the  $D$  meson contains a charm quark, the latter one being created exclusively in the primary scatterings, at the very first moment of the collision. In Fig. 18, we plot the normalized  $D$  me-

reference curve, which is the dashed black line representing identical multiplicity dependence for  $D$  mesons and charged particles. Considering the EPOS results without hydro (green lines), for low  $p_t$  (1-2 GeV/c) the curve is slightly above the reference, but with increasing  $p_t$  the green curves get steeper, which is due to the fact that with increasing multiplicity the saturation scale increases, and the events get harder, producing more easily both high  $p_t$  and charmed particles. Considering EPOS with hydro (red curves), the increase compared to the green curves is much stronger, which is due to the fact that “turning on hydro” will reduce the multiplicity (the available energy is partly transformed into flow). The red curves are close to the experimental data, both showing a much stronger increase compared to the reference curve, with the effect getting bigger with increasing  $p_t$ . So we may conclude this paragraph: to get these final results (the strong increase), two phenomena are crucial, namely, saturation which makes high multiplicity events harder, and the “hydro effect” which reduces multiplicity and “compresses” the multiplicity axis.

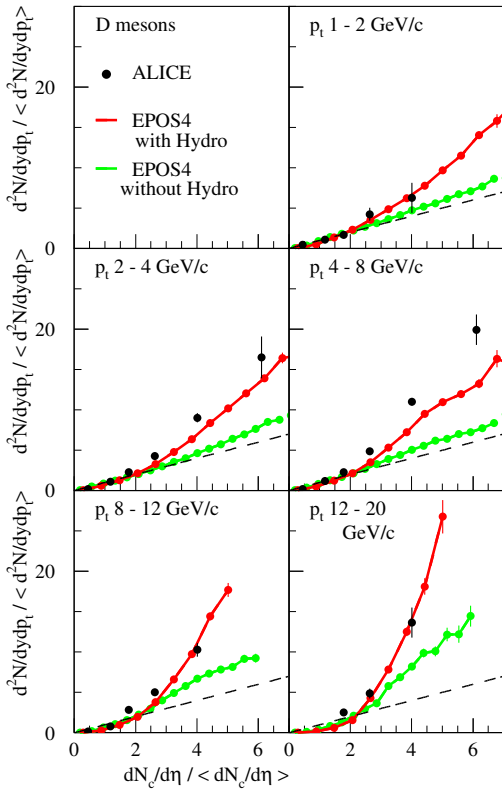


**Figure 18:** Normalized  $D$  meson multiplicity as a function of the normalized charged particle multiplicity for different  $p_t$  ranges in pp scattering at 7 TeV. We show EPOS results with and without hydro, compared to ALICE data.

son multiplicity ( $\frac{d^2N}{dydp_t} / \langle \frac{d^2N}{dydp_t} \rangle$ ) as a function of the normalized charged particle multiplicity ( $\frac{d^2N_c}{dydp_t} / \langle \frac{d^2N_c}{dydp_t} \rangle$ ) for different  $p_t$  ranges in pp scattering at 7 TeV, compared to ALICE data [46]. It is interesting to see in which way the simulations and the data deviate from the ref-

## 5 Charmed hadrons

Having already discussed the multiplicity dependence of charm production in the last chapter, we will show here some basic charm results (a detailed discussion will follow soon in a dedicated paper). We consider here just primary interactions, no hydro and no hadronic cascade, so the charm quarks originate from cut Pomeron, more precisely from the parton ladder. Cut parton ladders correspond in general to two chains of partons  $q - g - \dots - g - \bar{q}$  identified as kinky strings, with  $q$  referring to light flavor partons, and  $g$  to gluons. The Born process or branchings in the space-like or the time-like cascade may lead to  $Q\bar{Q}$  production, where  $Q$  refers to “heavy flavor” (HF) quarks, i.e. charm or bottom. In this case, we end up with parton chains of the type  $q - g - \dots - g - \bar{Q}$  and  $Q - g - \dots - g - q$ , which will decay (among others) into HF hadrons. In Fig. 19, we show transverse momentum spectra of  $c$  quarks (upper left),  $D^+$ ,  $D^-$  mesons (upper right),  $D^0$  mesons (lower left), and  $D^{*+}$ ,  $D^{*-}$  mesons (lower right) in pp collisions at 7 TeV. The red lines refer to EPOS simulations, the green points to FONLL calculations [47], and the black points to ALICE data [48]. In Fig. 20, we plot transverse momentum spectra of  $\Lambda_c$  and  $\Xi_c$  baryons (upper panel) and their ratio with respect to  $D^0$  mesons in pp collisions at 5 TeV. The red lines refer to EPOS simulations, and the black points to ALICE data [49, 50]. The production of charmed baryons is in principle straightforward, they are also coming from  $q - g - \dots - g - \bar{Q}$  and  $Q - g - \dots - g - q$  strings (with  $Q$  being a  $c$  quark in this case). The only difference compared to charmed meson production is the fact that here a diquark-antidiquark breakup occurs, which results in an essentially flat baryon / meson ratio, whereas the data show an increase towards small  $p_t$ . A similar

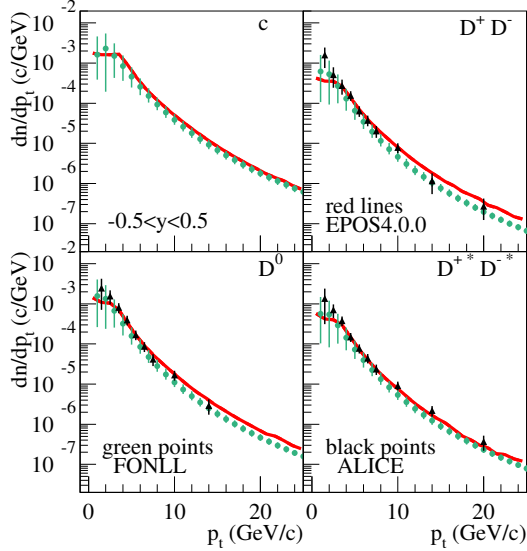


**Figure 19:** Transverse momentum spectra of  $c$  quarks and charmed mesons in pp at 7 TeV.

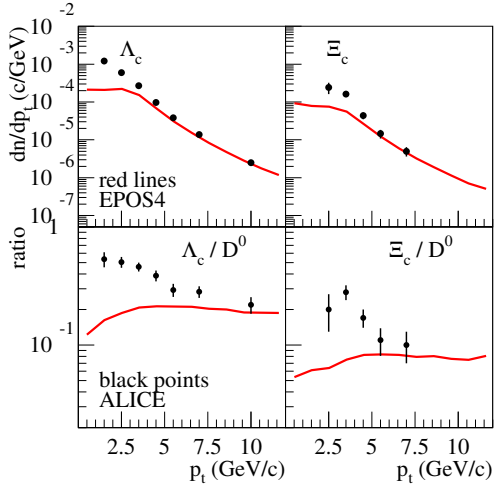


**Figure 20:** Transverse momentum spectra of charmed baryons in pp at 5.02 TeV.

“baryon/meson enhancement” in the region around 2 - 6 GeV/c has already been observed in the light flavor sector, where one possible explanation is collective flow.

Since we are producing charm (as everything else) in an event-by-event manner, we produce for each charm quark the corresponding charm antiquark, and depending on the production details they have characteristic correlations, which are also visible in  $D$  meson pair correlations. In Fig. 21, we show two-hadron correlations for  $D^0 D^0$  (upper left plot),  $D^0 \bar{D}^0$  (upper right),  $D^+ D^-$  (lower left), and  $D^+ D_s^-$  (lower right) as a function of the rapidity difference  $\Delta y$  in pp collisions at 7 TeV, with  $p_t$  values between 3 and 12 GeV/c and rapidities between 2 and 4. Red lines represent EPOS4 simulations and black dots data from LHCb [51]. In Fig. 22, we plot the correlations of these pairs as a function of the azimuthal angle difference  $\Delta\phi$ , again compared to LHCb.

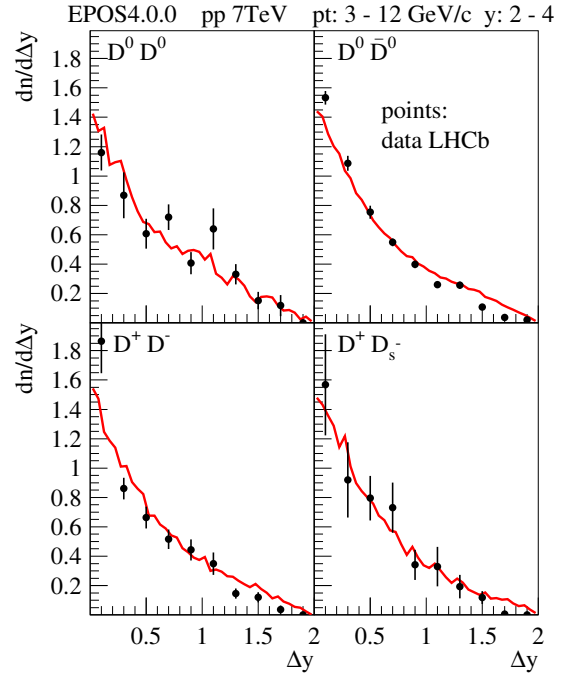


**Figure 21:** Two hadron correlations for  $D^0 D^0$ ,  $D^0 \bar{D}^0$ ,  $D^+ D^-$ , and  $D^+ D_s^-$  as a function of the rapidity difference  $\Delta y$  in pp collisions at 7 TeV. Red lines represent EPOS4 simulations and black dots data from LHCb.

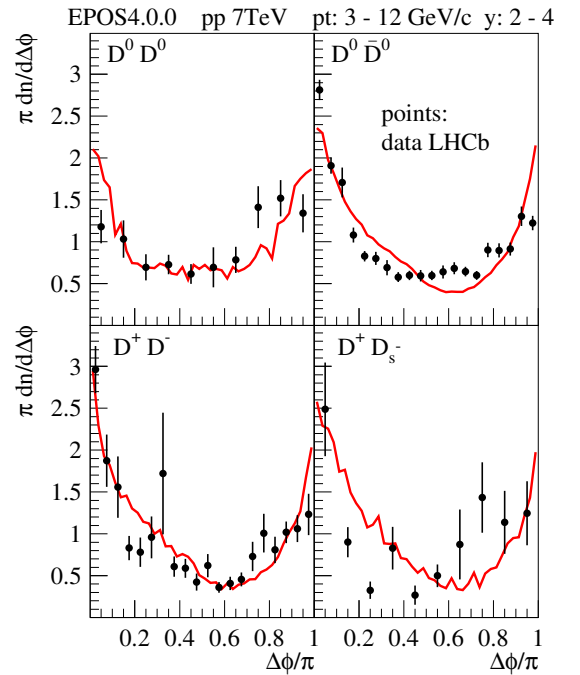


**Figure 22:** Two hadron correlations for  $D^0 D^0$ ,  $D^0 \bar{D}^0$ ,  $D^+ D^-$ , and  $D^+ D_s^-$  as a function of the azimuthal angle difference  $\Delta\phi$  in pp collisions at 7 TeV. Red lines represent EPOS4 simulations and black dots data from LHCb.

It should be noted that  $D^0 D^0$  represents a  $c - c$  correlations, whereas the three other combinations  $D^0 \bar{D}^0$ ,

$D^+D^-$ , and  $D^+D_s^-$  represent  $c - \bar{c}$  correlations. For the latter ones, the situation is quite simple: the  $c$  and the  $\bar{c}$  are always produced as pair from the same process, and therefore we expect them to be close in rapidity, with a preference of  $\Delta\phi = 0$  (in case of a time-like  $g \rightarrow c\bar{c}$ ), or at  $\Delta\phi = \pi$  in case of a Born process  $gg \rightarrow c\bar{c}$ . This is precisely what we see: The rapidity correlations have maxima at  $\Delta y = 0$  and then drop quickly, the  $\Delta\phi$  correlations have maxima at  $\Delta\phi = 0$  and  $\Delta\phi = \pi$ , observed in both EPOS4 simulations and data.

Surprisingly, the  $D^0D^0$  correlations (corresponding to a  $c - c$  pair) look very similar, which suggests that also  $c - c$  pairs originate from the same process, like a timelike  $g \rightarrow gg \rightarrow c\bar{c}c\bar{c}$  or a Born process  $gg \rightarrow gg$  followed by  $g \rightarrow c\bar{c}$ ,  $g \rightarrow c\bar{c}$ .

Since EPOS4 creates charm always in terms of  $c - \bar{c}$  pairs, it is quite tempting to look into the possibility to produce charmonium. Easy to implement is the idea of the color evaporation model [52, 53, 54], where charmonium is created with a certain probability in case of a  $c - \bar{c}$  pairs being in the appropriate mass range. So we consider all  $c - \bar{c}$  pairs from the same Pomeron (fully evaluated, including time-like emissions), and compute the invariant mass  $M_{c\bar{c}}$ . Whenever this mass is less than the sum of two  $D$  meson masses and bigger than the  $J/\Psi$  mass, the  $c - \bar{c}$  pair is with a certain probability  $w_{J/\Psi}$  considered to be a  $J/\Psi$ . In Fig. 23, we plot prompt  $J/\Psi$

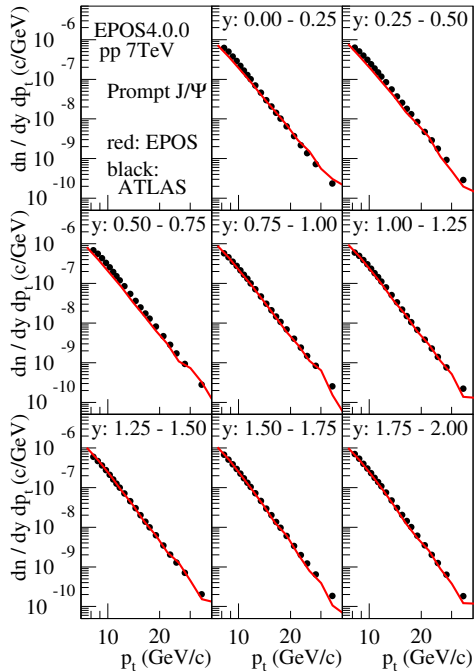


Figure 23: xxx.

(not coming from beauty decays) from EPOS4 simulations compared to ATLAS data [55].

## 6 Summary

We reported on new ideas, implemented in EPOS4, which provide a new understanding of a deep connection between four basic concepts in pp and AA collisions: parallel scattering, energy conservation, factorization, and saturation. It is mandatory to treat multiple scatterings in parallel, and a “natural” framework is S-matrix theory, with an S-matrix being given as a product of several entities representing individual scatterings, referred to as Pomerons. We recalled that neglecting energy conservation leads perfectly to factorization, but also for soft processes, contradicted by data. On the other hand, considering energy conservation, and identifying the cut Pomeron expression  $G$  with the parton ladder result  $G_{\text{QCD}}$  (as done in earlier EPOS versions), one completely spoils factorization, also for hard processes, again contradicted by data.

We have shown that the problem is due to a “deformation” of the energy distribution of Pomerons in case of multiple parallel scatterings, namely the probability to carry a large fraction of the total energy is reduced, which is unavoidable. The solution of the problem has been shown to be a dynamical saturation scale, such that the cut Pomeron expression  $G$  is equal to  $k \times G_{\text{QCD}}(Q_{\text{sat}}^2)$  with  $k$  being inversely proportional to the deformation. In this case factorization is recovered, but only for hard processes as it should be. For example, a large number of parallel scatterings will not affect high  $p_t$  particle production, it will only make the saturation scale big and thus suppress small  $p_t$  particle production.

In our new formalism, the full multiple scattering scenario converges to the single Pomeron result in case of inclusive cross sections (factorization), which allows using the single Pomeron (or factorization) mode, based on EPOS parton distribution functions. So we can now, with the same formalism, treat extremely high  $p_t$  particle production in factorization mode, and as well collective effects in high multiplicity events using the full simulation.

We discussed several examples, essentially multiplicity dependencies (of particle ratios, mean  $p_t$ , charm production) which are very strongly affected by the saturation issues discussed in this paper and core-corona effects mixing flow (being very strong) and non-flow contributions.

## References

- [1] D. Gross and F. Wilczek, Physical Review Letters **30**, 1343 (1973).
- [2] H. Politzer, Physical Review Letters **30**, 1346 (1973).
- [3] J. Collins, D. Soper, and G. Sterman, in Perturbative Quantum Chromodynamics, edited by A.H. Mueller, World Scientific, Singapore (1989).

- [4] R. Ellis, W. Stirling, and B. Webber, in *QCD and Collider Physics*, Cambridge Monographs on Particle Physics, Nuclear Physics and Cosmology (1996).
- [5] CMS, V. Khachatryan *et al.*, *JHEP* **09**, 091 (2010), 1009.4122.
- [6] V. N. Gribov and L. N. Lipatov, *Sov. J. Nucl. Phys.* **15**, 438 (1972).
- [7] G. Altarelli and G. Parisi, *Nuclear Physics B.* **126**, 298 (1977).
- [8] Y. L. Dokshitzer, *Sov. Phys. JETP* **46**, 641 (1977).
- [9] L. V. Gribov, E. M. Levin, and M. G. Ryskin, *Phys. Rept.* **100**, 1 (1983).
- [10] L. D. McLerran and R. Venugopalan, *Phys. Rev. D* **49**, 2233 (1994), hep-ph/9309289.
- [11] L. D. McLerran and R. Venugopalan, *Phys. Rev. D* **49**, 3352 (1994), hep-ph/9311205.
- [12] A. Kovner, L. McLerran, and H. Weigert, *Phys. Rev.* **D52**, 3809 (1995), hep-ph/9505320.
- [13] Y. V. Kovchegov, *Phys. Rev.* **D54**, 5463 (1996), hep-ph/9605446.
- [14] Y. V. Kovchegov, *Phys. Rev.* **D55**, 5445 (1997), hep-ph/9701229.
- [15] Y. V. Kovchegov and D. H. Rischke, *Phys. Rev.* **C56**, 1084 (1997), hep-ph/9704201.
- [16] J. Jalilian-Marian, A. Kovner, L. McLerran, and H. Weigert, *Phys. Rev.* **D55**, 5414 (1997), hep-ph/9606337.
- [17] J. Jalilian-Marian, A. Kovner, A. Leonidov, and H. Weigert, *Nucl. Phys.* **B504**, 415 (1997), hep-ph/9701284.
- [18] Y. V. Kovchegov and A. H. Mueller, *Nucl. Phys.* **B529**, 451 (1998), hep-ph/9802440.
- [19] A. Krasnitz and R. Venugopalan, *Nucl. Phys.* **B557**, 237 (1999), hep-ph/9809433.
- [20] J. Jalilian-Marian, A. Kovner, A. Leonidov, and H. Weigert, *Phys. Rev.* **D59**, 034007 (1999), hep-ph/9807462.
- [21] J. Jalilian-Marian, A. Kovner, and H. Weigert, *Phys. Rev.* **D59**, 014015 (1999), hep-ph/9709432.
- [22] J. Jalilian-Marian, A. Kovner, A. Leonidov, and H. Weigert, *Phys. Rev.* **D59**, 014014 (1999), hep-ph/9706377.
- [23] H. J. Drescher, M. Hladik, S. Ostapchenko, T. Pierog, and K. Werner, *Phys. Rept.* **350**, 93 (2001), hep-ph/0007198.
- [24] V. N. Gribov, *Zh. Eksp. Teor. Fiz.* **53**, 654 (1967).
- [25] V. N. Gribov, *Sov. Phys. JETP* **29**, 483 (1969).
- [26] V. A. Abramovsky, V. N. Gribov, and O. V. Kancheli, *Yad. Fiz.* **18**, 595 (1973).
- [27] T. Pierog, I. Karpenko, J. M. Katzy, E. Yatsenko, and K. Werner, *Physical Review C* **92** (2015).
- [28] K. Werner, B. Guiot, I. Karpenko, and T. Pierog, *J. Phys. Conf. Ser.* **458**, 012020 (2013).
- [29] T. Pierog and K. Werner, *Acta Phys. Polon. Supp.* **8**, 1031 (2015).
- [30] S. Dulat *et al.*, *Physical Review D* **93** (2016).
- [31] ZEUS, M. Derrick *et al.*, *Z. Phys.* **C72**, 399 (1996), hep-ex/9607002.
- [32] H1 Collaboration, Abt *et al.*, *Z. Phys.* **C63**, 377 (1994).
- [33] H1 Collaboration, Aid *et al.*, *Nucl. Phys.* **B470**, 3 (1996).
- [34] H1 Collaboration, Adlhoff *et al.*, *Nucl. Phys.* **B485**, 3 (1996).
- [35] ATLAS, M. Aaboud *et al.*, *JHEP* **05**, 195 (2018), 1711.02692.
- [36] K. Werner, *Phys. Rev. Lett.* **98**, 152301 (2007), 0704.1270.
- [37] K. Werner, I. Karpenko, T. Pierog, M. Bleicher, and K. Mikhailov, *Phys. Rev. C* **82**, 044904 (2010), 1004.0805.
- [38] K. Werner, B. Guiot, I. Karpenko, and T. Pierog, *Phys. Rev. C* **89**, 064903 (2014), 1312.1233.
- [39] S. A. Bass *et al.*, *Prog. Part. Nucl. Phys.* **41**, 225 (1998), nucl-th/9803035.
- [40] M. Bleicher *et al.*, *J. Phys.* **G25**, 1859 (1999), hep-ph/9909407.
- [41] ALICE, J. Adam *et al.*, *Nature Phys.* **13**, 535 (2017), 1606.07424.
- [42] ALICE, B. B. Abelev *et al.*, *Phys. Lett. B* **728**, 216 (2014), 1307.5543, [Erratum: *Phys.Lett.B* 734, 409–410 (2014)].
- [43] ALICE, B. Abelev *et al.*, *Phys. Rev. C* **88**, 044910 (2013), 1303.0737.
- [44] ALICE, B. B. Abelev *et al.*, *Phys. Rev. Lett.* **111**, 222301 (2013), 1307.5530.
- [45] ALICE, J. Adam *et al.*, *Eur. Phys. J. C* **75**, 226 (2015), 1504.00024.
- [46] ALICE, J. Adam *et al.*, *JHEP* **09**, 148 (2015), 1505.00664.

- [47] M. Cacciari *et al.*, JHEP **10**, 137 (2012), 1205.6344.
- [48] ALICE, B. Abelev *et al.*, JHEP **01**, 128 (2012), 1111.1553.
- [49] ALICE, S. Acharya *et al.*, Phys. Rev. Lett. **127**, 202301 (2021), 2011.06078.
- [50] ALICE, S. Acharya *et al.*, JHEP **10**, 159 (2021), 2105.05616.
- [51] LHCb, R. Aaij *et al.*, JHEP **06**, 141 (2012), 1205.0975, [Addendum: JHEP 03, 108 (2014)].
- [52] V. Barger, W. Keung, and R. Phillips, Physics Letters B **91**, 253 (1980).
- [53] R. Gavai *et al.*, Int. J. Mod. Phys. A **10**, 3043 (1995), hep-ph/9502270.
- [54] Y.-Q. Ma and R. Vogt, Phys. Rev. D **94**, 114029 (2016).
- [55] ATLAS, G. Aad *et al.*, Eur. Phys. J. C **76**, 283 (2016), 1512.03657.